Hindawi
International Journal of Antennas and Propagation
Volume 2019, Article ID 6202095, 19 pages
https://doi.org/10.1155/2019/6202095

Research Article

Determination of an Indoor Target Position: An Accurate and Adaptable Approach Based on Differential Positioning

Siye Wang,[1,2,3] **Chang Ding**,[4] **Weiqing Huang**,[1,2,3] **Yanfang Zhang**,[2,3] **Jianguo Jiang**,[1,2,3] **Shaoyi Zhu**,[2,3] **Yue Cui**,[2,3] **and Jun-yu Lin**[2,3]

[1]*School of Computer and Information Technology, Beijing Jiaotong University, Beijing, China*
[2]*Institute of Information Engineering, Chinese Academy of Sciences, Beijing, China*
[3]*School of Cyber Security, University of Chinese Academy of Sciences, Beijing, China*
[4]*National Security Science and Technology Evaluation Center, Beijing, China*

Correspondence should be addressed to Siye Wang; wangsiye@iie.ac.cn

Received 23 June 2019; Revised 24 September 2019; Accepted 11 November 2019; Published 13 December 2019

Academic Editor: Giuseppina Monti

The growing demand for new products that rely on the accurate identification of a target's location indoors, while remaining mindful of cost, continues to drive research in this important and challenging area. Researchers are actively pursuing algorithmic improvements to eliminate errors introduced from complex interference factors present in indoor, wireless communication environments. In this work, we adopt a differential signal strength method in the design of our new indoor localization algorithm. The proposed algorithm reduces errors in the time domain by smoothing out the wireless signal fluctuations, thus stabilizing the signal; a single exponential algorithm is applied to the signal strength parameters collected to accomplish this. The target's position is then computed by utilizing both the plane geometric method and difference localization theory. This combination of techniques is reasonable for the environment under consideration (small scale, wireless), as the multipath effects for the signal are approximately equal under these conditions. In addition, the proposed approach is compatible with a wide variety of technologies (e.g., RFID and Bluetooth); it can be cost-effectively deployed by leveraging an existing hardware infrastructure. The proposed approach has been implemented and experimentally validated. The test results are very promising: they indicate that our algorithm improves the positioning accuracy by 70%–80% in comparison with the trilateration and LANDMARC positioning algorithms.

1. Introduction

The ability to accurately determine the position of a device, and more recently a user with a device, in an indoor environment remains an important and challenging research problem. This is a fundamental feature across a wide and growing variety of fields with significant social and economic importance (e.g., emergency rescue, disaster prevention, logistics management, and device testing). The availability of advanced mobile networks, intelligent devices, and the Internet of things continues to drive the demand for sophisticated location-based services for indoor applications. Many people spend a substantial amount of time indoors, 87%, with high levels of mobile phone use for voice and data (refer to Figure 1). Hence, the indoor positioning technology is of broad interest [1].

Although GPS and other GNSS technologies can solve the problem of outdoor localization well, the satellite signal strength and signal quality decline rapidly in an indoor or sheltered environment. The signal strength and the quality of an indoor cellular mobile network are better than those of a satellite in the same condition, but the localization accuracy of the cellular mobile network is poor because of limited bandwidth. Usually, the localization accuracy of a cellular mobile network ranges from several decameters to several hundred meters [2, 3].

Consequently, alternatives to GPS and GNSS are needed to provide accurate indoor positioning technology. The

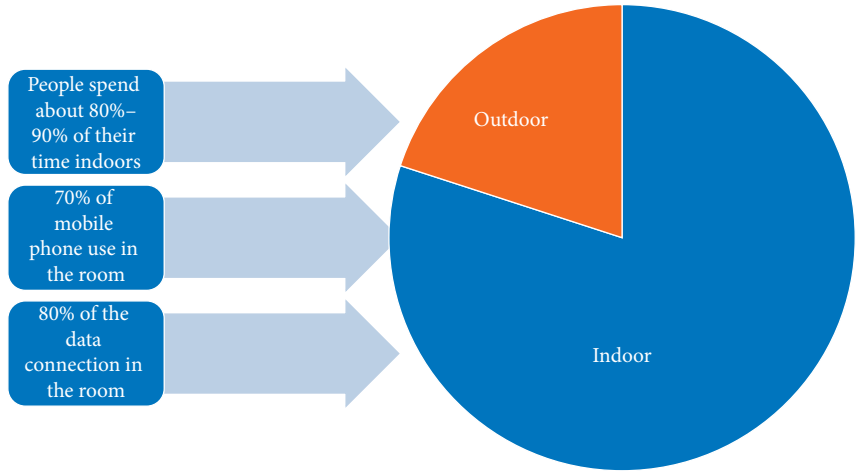

Figure 1: Distribution of people's activities: indoor and outdoor environments.

problem is challenging, however, due to the variations in rooms (size, shape, and construction materials) and their content (furniture and artwork installations). Barriers introduce signal diffraction, refraction, and scattering, which modify the signal characteristics (strength, phase, and amplitude), and introduce a multipath effect.

An established solution is to first having the transmitter estimate the distance to the target with a receive signal strength indicator (RSSI); the target location is subsequently computed. However, the RSSI does not exhibit a decreasing linear response as distance increases, which limits its accuracy. The nonlinear response is due to small-scale shadow fading, resulting from the multipath transmission. After analyzing the factors influencing the accuracy of localization in indoor, wireless network environments, the essential research question emerges: Can a more accurate algorithm be designed, which reduces both the propagation error and the multipath effect? [4].

In this work, we propose the design, implementation, and validation for a novel localization algorithm for indoor, wireless network environments. The main contributions of our paper are as follows:

(1) Both the plane geometric method and difference localization theory are used in the design of a novel indoor localization algorithm. This combination of techniques is reasonable for the environment under consideration (small scale, wireless), as the multipath effects for signals are approximately equal under these conditions.

(2) The proposed algorithm is designed to reduce errors in both the time and space domains. For time, the acquired signal is treated with an exponential smoothing method to reduce fluctuations over time, creating a more stable signal. For space, the error introduced by the propagation multipath effect is addressed using differential positioning methods. The algorithm is demonstrated in an empirical study with complex environments to be more accurate than other currently available alternatives, achieving an accuracy of 0.65 m.

(3) The algorithm adapts well to widely available location technologies (e.g., Bluetooth and RFID). This feature has the potential to support lower-cost deployments, by reusing the existing hardware infrastructure.

The remainder of this paper is organized as follows: Section 2 presents an overview of current indoor localization algorithms. The signal propagation model and errors introduced by the multipath effect in indoor, wireless network environments are described in Section 3. The error reduction method, addressing the multipath effect in both time and space domains, is presented in Section 4. The underlying theory for our differential positioning algorithm is presented in Section 5, along with its implementation and calculation methods. The validation results for a comparative empirical study are presented in Section 6. Lastly, a summary of the results and direction for the future work are presented in Section 7.

2. Related Works

2.1. The Kinds of the Indoor Positioning Algorithms. There are several types of technologies used for indoor positioning, such as infrared-based indoor positioning technology [5], ultrasonic-based indoor positioning technology [6, 7], Bluetooth-based indoor positioning technology [8], ZigBee-based indoor positioning technology [9], WiFi-based indoor positioning technology [10, 11], cellular-based indoor positioning technology [12], UWB-based indoor positioning technology [13, 14], inertial navigation-based indoor positioning technology [15, 16], and RFID-based indoor positioning technology.

Generally, these technologies rely on one or more sensing signals to calculate positions. For example, the distance can be represented by the received signal strength and the arrival time of the received signal. The stronger the received signal is, the closer the signal sender is. Similarly, the earlier the signal arrives, the closer the receiving position is to the transmitting position of the signal. When there is only one received signal, the location cannot be calculated.

When there are multiple devices for receiving the signal, the location can be calculated.

According to the different processing methods of measurement parameters, indoor positioning algorithms can be divided into triangulation-based positioning algorithms and scene-based positioning algorithms.

(1) Triangulation-based positioning algorithm: this kind of algorithm always makes use of the characteristics of the arrival signals, such as arrival time, phase, and strength. The differences in time and phase help in positioning a tag.

As shown in Figure 2, the SpotON system is a typical representative of this type of algorithm, proposed by Hightower et al. [17]. The system uses three or more readers as the base stations to record the signal strength of each tag read by the reader and calculate the position of the tag by means of triangulation. Later, a modified SpotON system based on ad hoc [18] introduced the ad hoc network into the SpotON positioning method. In contrast, the TOA algorithm depends on the time of arrival. The principle diagram of the TOA algorithm is shown in Figure 3. First, the target distance from the receiving antenna based on the propagation time of the signal arriving at the receiving antenna is found, and then the triangulation principle is used to find the target coordinates. Bao and Wang used the arrival time method to track the motion trajectory of the person [19]. Wang and Shen used the L-MUSIC method to locate the label using the arrival time method [20]. Studies on the TOA method applied to SAW-RFID positioning are also available [21, 22]. There are some disadvantages in using TOA in the RFID positioning system: since the indoor positioning scene is usually small, the distance from the tag to the reader is close, and the short-distance ranging is required to be high with the propagation speed of the electromagnetic wave in the air. Time accuracy, meanwhile, requires the transmitter and receiver to remain accurately synchronized; the relatively low communication rate of the wireless device makes it difficult to add an accurate time stamp.

(2) Scene analysis-based positioning mechanism: first, the scene parameter information is collected, then the detected target information is matched with the scene information, and finally the target is located accordingly. The typical scene analysis-based positioning algorithms are the reference tag method, fingerprint positioning method, centroid algorithm, and neighbor node method.

The LANDMARC algorithm uses a mix of fixed reference tags, fixed readers, and target reference tags [23]. The indoor space is arranged with a collection of fixed readers and a large number of fixed reference tags. The fixed readers compute the signal strength of the fixed and target reference tags; the position of the target tag can be computed. Since then, many scholars have conducted follow-up studies on

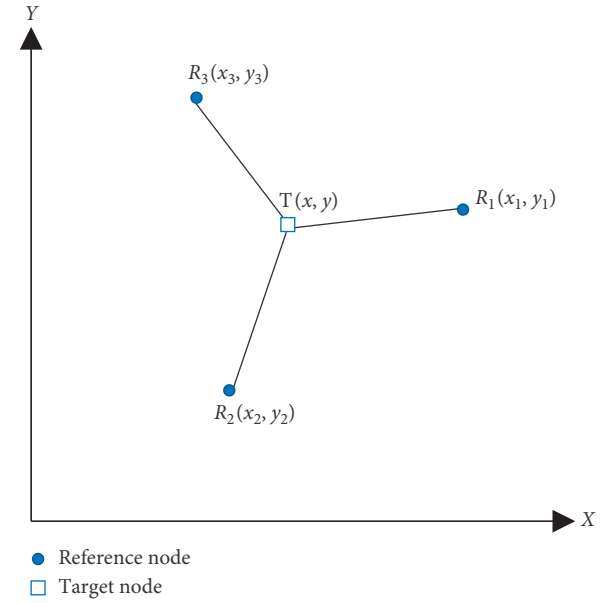

Figure 2: Overview of the SpotON system.

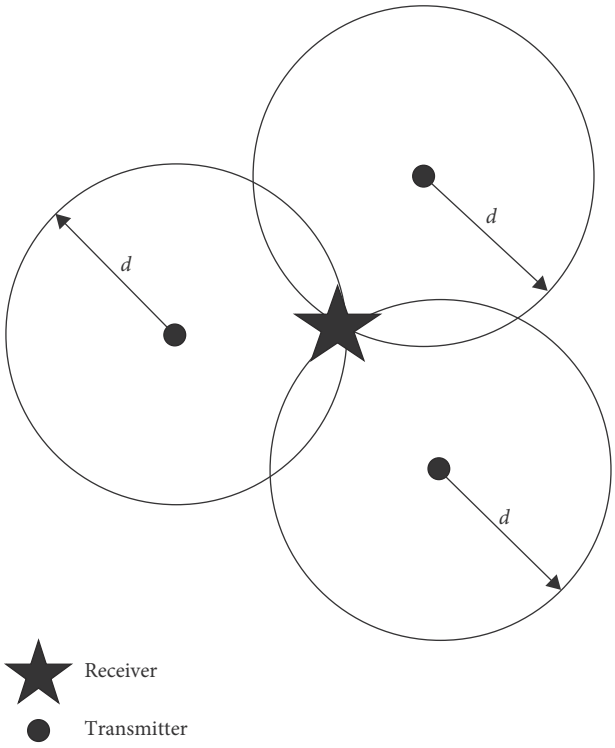

Figure 3: TOA algorithm.

the LANDMARC system and have proposed various improvements. Jin et al. introduced the concept of neighbor nodes in the LANDMARC system to improve the efficiency of positioning [24]. Chattopadhyay and Harish conducted a large number of experiments on the LANDMARC system, quantitatively analysed the arrangement and density of the reference tags, and pointed out the positioning effect of the LANDMARC system. This approach is sensitive to the tags' orientations; it requires the tags to be aligned in the same

direction [25]. This team used neural networks to improve the LANDMARC system, trained the neural network through the signal strength of prearranged target and reference tags, and used trained neural networks to calculate the location of unknown target tags [26]. Choi et al. introduced a signal strength correction method that uses the corrected signal strengths of the target tag and the reference tag to calculate and improve the accuracy of positioning [27]. Zhao et al. proposed a VIRE (virtual reference elimination) algorithm based on a virtual reference tag. It estimates the location information and signal strength of the virtual reference tag by combining the position information and signal strength of the actual reference tag with a linear interpolation method to achieve indoor transmission [28]. Xu et al. [29] proposed an algorithm based on support vector regression to further improve the positioning accuracy of LANDMARC, and the experimental result shows that the RMSE is about 20.2 cm. Xu et al. [30] then proposed an algorithm, called the BKNN, based on the K-nearest neighbor and Bayesian probability. The average location estimation error was further reduced to approximately 15 cm.

2.2. The Evaluation Indicators of Indoor Positioning Algorithms. The evaluation of performance of positioning algorithms in the indoor environment has been considered from numerous perspectives. The commonly used indoor target positioning algorithm performance evaluation indicators are as follows:

(1) *Positioning Accuracy*. This is the most important and commonly used index in positioning algorithm evaluation. In the target positioning system, the positioning accuracy generally refers to the deviation of the actual position of the target from the estimated position.

(2) *Environmental Adaptability*. Positioning capability refers to both the number of targets that the algorithm can locate at the same time and the scenario to which the algorithm applies.

(3) *Real-Time Performance*. It usually includes the positioning algorithm's computation time, as well as the installation and configuration time of the system. It is an important criterion for evaluating the positioning algorithm. For indoor sports goals, real-time and quick acquisition of target locations is of great value to the actual application of the system.

(4) *Power Consumption*. This is the factor that has the most influence on the design and implementation of the algorithm. Different algorithms have different complexity, and the number of positioning devices that need to participate in positioning is also different; in addition, the energy of positioning tags is very limited. Therefore, under the requirement of satisfying the positioning accuracy, an algorithm with less communication overhead, less computation, and less storage overhead should be selected.

(5) *Implementation Complexity and Cost*. Implementation complexity is an important criterion for judging the merits of a positioning algorithm. Algorithms with high positioning accuracy but complex implementation are often not used. The implementation cost is mainly the total cost of the infrastructure, additional hardware, and other equipment required for the specified algorithm, and the low-cost location algorithm should be selected under the guarantee of positioning accuracy and limited funds.

The comparison of positioning algorithms with respect to these evaluation indicators is summarized in Table 1; the qualitative values used are poor, fair, good, and very good.

Although indoor location technology has made considerable progress, the application deployment of location technology is still complex. Meanwhile, the target's physical properties, the electromagnetic environment interference, and moving items all can influence the location results directly. Therefore, indoor location technology has a wide space for improvement [31].

3. Signal Modelling and Error Analysis for Indoor, Wireless Network Environments

3.1. Signal Propagation Model. In an indoor environment, the transmission loss of electromagnetic waves can be represented using the lognormal shadowing model, when interference is not considered:

$$\mathrm{PL}(d_0) = 10n\log_{10}\frac{G_tG_r\lambda^2}{(4\pi)^2d_0^2}. \tag{1}$$

In this model, $\mathrm{PL}(d_0)$ is the power density loss of a received signal from the distance d_0. The gain of the receiving and transmitting antennas is G_r and G_t, respectively. The additional parameters include the environment factor n and the signal wavelength λ; the distance d_0 is typically recommended to be 1 m [10].

More generally, power density loss of a signal over a distance d is

$$\mathrm{PL}(d) = \mathrm{PL}(d_0) + 10n\log_{\{10\}}[d/d_0] + X_{\{\sigma\}}, \tag{2}$$

where X_σ is the normal distribution $\mathcal{N}(\mu, \sigma^2)$ such that σ ranges within [4, 10] [32].

$$\mathrm{Pr}(d) = \mathrm{Pt} - \mathrm{PL}(d). \tag{3}$$

From (3), it is obvious that the receiving power equals transmitting power minus loss power. A straightforward substitution of (2) into (3) results in the calculation of the received signal strength $\mathrm{Pr}(d_0)$ for the distance d as

$$\mathrm{Pr}(d) = \mathrm{Pr}(d_0) - 10n\log 10\frac{d}{d_0} - X_\sigma. \tag{4}$$

Hence, (4) indicates the power strength of the received signal, under ideal conditions, behaves as a logarithmic function, where the received power decreases as the transmission distance increases. The RSSI is adopted in our experiments as an approximation of $\mathrm{Pr}(d_0)$, as a simplifying assumption. However, this adoption does introduce some

Table 1: Comparison of evaluation indicators for indoor positioning algorithms.

Algorithm	Accuracy	Real-time response	Adaptability	Power efficiency	Cost
TOA	Very good	Poor	Poor	Good	Good
LANDMARC	Very good	Very good	Very good	Fair	Good

error, and measured RSSI values in indoor environments fluctuate (refer to Figure 4).

3.2. Signal Error Analysis. In actual environments, especially indoor, electromagnetic signal propagation encounters obstacles (e.g., furniture), which interfere with their transmissions. These encounters introduce reflection, diffraction, and scattering of the signals; as a result, equation (1) no longer models the transmission correctly. A very small change in the position of a moving target can cause signal fluctuations because the received composite signal contains signal components that are reflected from different directions by different reflection sources, as well as diffracted and scattered signal components.

When there is a sharp obstacle on a transmission path between the signal receiving antenna and the signal emitting source, the signal is often diffracted, and a secondary wave generated from the blocking surface is transmitted to the obstacle. The diffraction of the RF signal is affected by many factors including the polarization, phase, and amplitude of the signal, as well as the diffraction spot's shape on the obstacle. When there are a large number of small-sized (i.e., less than the wavelength) objects in the propagation medium, scattering occurs during signal propagation. Scattering is often caused by a rough surface, small objects, or some irregularly shaped objects. In reality, not only the surface of the metal but also the insulator can produce reflections. The reflection of electromagnetic waves from the surface of the insulator is complicated and there is no ideal metal surface, but even common insulating materials can produce reflections.

When the above phenomenon occurs simultaneously in an actual indoor propagation environment, the antenna receives all the signals arriving from different directions. In other words, it receives a vector sum of these signals; this is called the multipath effect. The multipath propagation caused by the reflection of the surface is also called specular multipath. The multipath propagation caused by diffraction and scattering is also called diffuse multipath.

Based on the above analysis, it can be seen that the fundamental factor that restricts the indoor wireless signal localization algorithm in the environment is that the interference of multipath effects in the wireless signal propagation process seriously affects the stability and reliability of the signal. As shown in Figure 5, the multipath effect is simplified, and the signal E_{TOT} received by the wireless signal receiver R is composed of two parts, the line-of-sight path signal $E_{\mathrm{LOS}d'}$ and the non-line-of-sight path signal E_g:

$$E_{\mathrm{TOT}} = E_{\mathrm{LOS}d'} + E_g. \tag{5}$$

As shown in Figure 5, let τ_d be the time delay of the phase difference between the line-distance path signal and the non-line-of-sight path signal electric field components. The calculation method is shown in (6). d is the distance between the transmitter and the receiver of the wireless signal, and $d\prime$ is the line-of-sight. Path distance, d'', is the multipath path distance, c is the speed of light, h_t is the height of the transmitter from the ground, and h_r is the height of the receiver from the ground.

$$\tau_d = \frac{d'' - d'}{c} \cong \frac{2h_t h_\gamma}{cd}. \tag{6}$$

Let the signal propagation time be t, then R receives the wireless signal, as shown in (7), where d_0 is the standard distance and E_0 is the received signal size at the standard distance.

$$E_{\mathrm{ror}}(d,t) = \frac{E_0 d_0}{d'}\cos\left(\omega\left(t - \frac{d'}{c}\right)\right) + (-1)\frac{E_0 d_0}{d''} \cdot \cos\left(\omega\left(t - \frac{d''}{c}\right)\right). \tag{7}$$

According to (6), when the distance $d > h_t + h_r$, the signal E_{TOT} is approximately

$$E_{\mathrm{ror}}(f,d) \cong \frac{2E_0 d_0}{d} \cdot \frac{2\pi f h_t h_r}{dc} = \frac{4\pi E_0 d_0 h_t h_r}{c} \cdot \frac{f}{d^2}. \tag{8}$$

Comparing (7) and (8), it can be seen that the effects of multipath propagation will lead to signal distortion. As a consequence of variable and complex indoor environments, dense multipath effects will be generated, thus making the median stability and reliability of the signal propagation process worse.

4. Indoor Wireless Signal Propagation Error Reduction Method

As mentioned in Section 3, fluctuations and interference may occur at different times and in different spaces. Therefore, this study focuses on eliminating interference and noise of the wireless signal from two aspects: time and space. We realize the reduction of the indoor wireless signal transmission error through the combination of the two aspects.

4.1. Wireless Signal Acquisition Error Reduction Method. Errors resulting from signal strength fluctuations over time are inherent in indoor, wireless network environments. Figure 6 illustrates a simple schematic of this situation, where the receiver acquires the wireless signal at the distance d.

Representing the collection of n data values in the time period T, the representative parameter, RSSI, for the signal strength parameter is

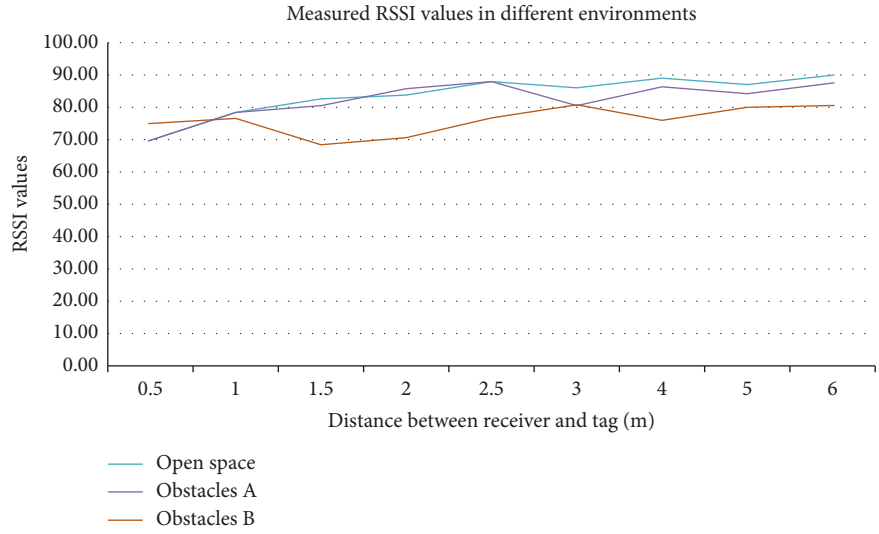

Figure 4: Multipath propagation environment: changes in received RFID signal strength vs. the distance.

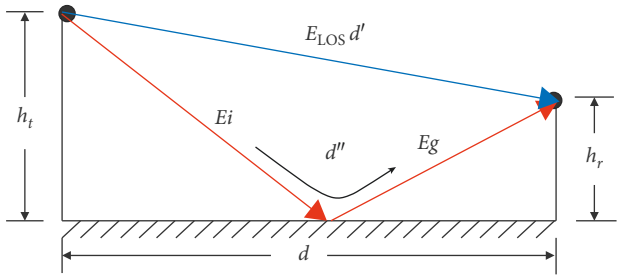

Figure 5: Multipath effect of indoor wireless signal transmission.

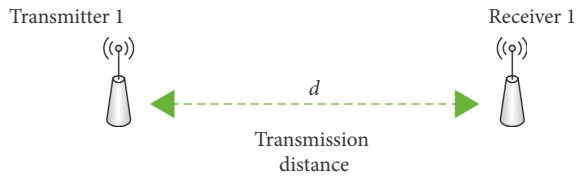

Figure 6: Schematic of signal transmitting and receiving.

$$\mathrm{RSSI}_i = \{\mathrm{RSSI}_1, \mathrm{RSSI}_2, \ldots, \mathrm{RSSI}_n\}. \quad (9)$$

When a single exponential smoothing algorithm is applied, the result is presented as

$$s_i = a\mathrm{RSSI}_i + (1-a)s_{i-1}, \quad (10)$$

where a is the smoothing factor and s_i is the accumulated value of the signal strength. The smoothing factor determines the weight of the currently observed signal strength in the final results. According to related conclusions, when there are data fluctuations, and the long-term variation trend is not obvious, the smoothing factor value ranges from 0.1 to 0.4. According to the transmission pattern of the indoor wireless signal, the smoothing factor should be within a small range to avoid the signal fluctuation and error. This study sets the single exponential smoothing factor value to be 0.25. When a smoothing algorithm is applied to a data series, the current smoothing value is affected by all of the formerly observed values; this effect progressively decreases. This method guarantees the forward integrity of the data and maintains a good data processing efficiency. The results of applying the smoothing algorithm are presented in Figure 7. In the time domain, the fluctuations of the signal strengths are remarkably reduced.

4.2. Wireless Signal Propagation Error Reduction Method. The essence of a distance measurement positioning algorithm is that the distance information between the receiver and the transmitter can be computed by using the signal strength. The accuracy of this computation is impacted by the multipath effect in wireless environments, as a result of reflection, diffraction, and interference in indoor settings. We begin with the definition of the signal strength reference attenuation δ:

$$\delta = \Pr(d_0) - \Pr(d). \quad (11)$$

According to (12), the expression of the relationship between the distance d and the reference attenuation δ is

$$d = 10^{(\delta - X_\sigma)/10n} d_0. \quad (12)$$

Solving the derivative of the distance d about δ results in

$$\frac{\partial d}{\partial \delta} = \frac{\ln 10}{10n} 10^{(\delta - X_\sigma)/10n} d_0. \quad (13)$$

The reference attenuation vector of signal strength received at n different positions is set as

$$\delta_i' = \delta_i^1 + \delta_\sigma^1, \delta_i^2 + \delta_\sigma^2, \ldots, \delta_i^n + \delta_\sigma^n. \quad (14)$$

The corresponding distance vector of each signal reference attenuation vector is

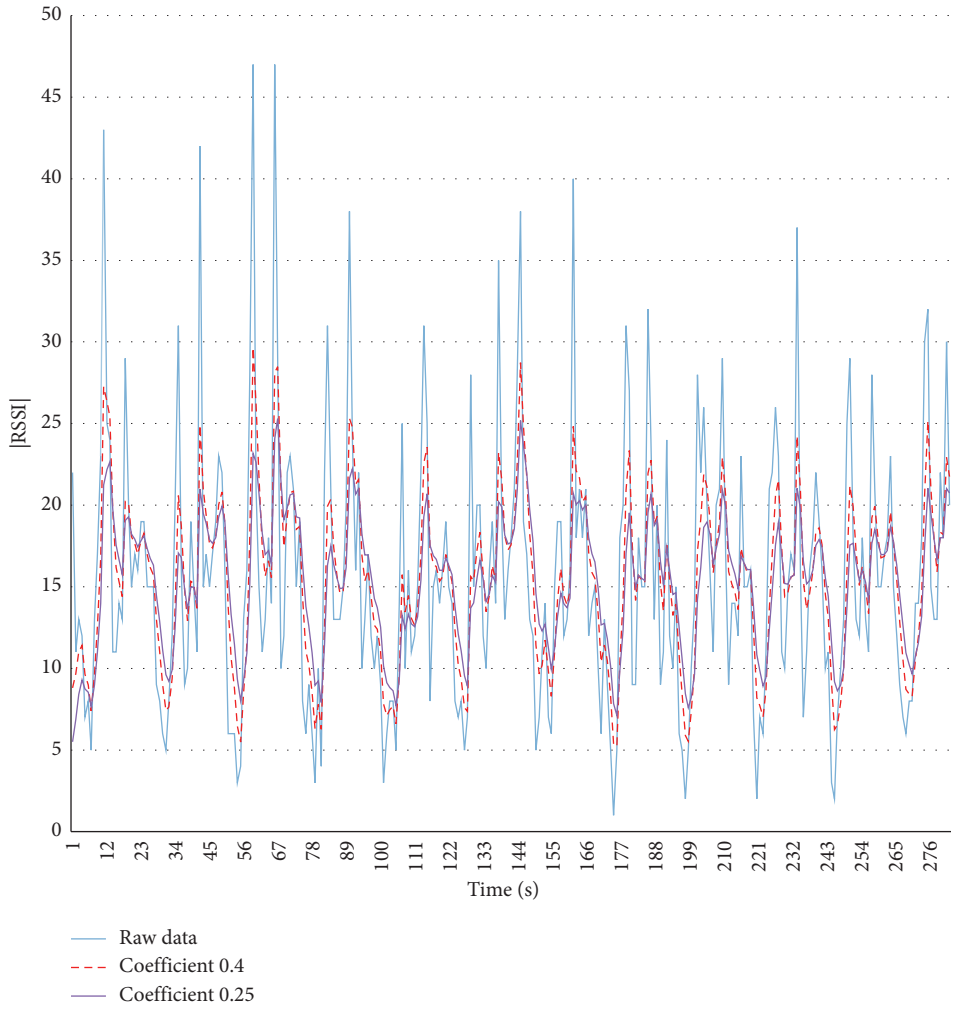

Figure 7: Effect of the single exponential smoothing method.

$$d_i' = \left(d_i^1 + d_\sigma^1, d_i^2 + d_\sigma^2, \ldots, d_i^n + d_\sigma^n\right), \tag{15}$$

where $d_\sigma = (d_\sigma^1, d_\sigma^2, \ldots, d_\sigma^n)$ is the distance vector error induced by the environment noise vector error $\delta_\sigma = (\delta_\sigma^1, \delta_\sigma^2, \ldots, \delta_\sigma^n)$ and $\varphi_i = \delta_i - X_\sigma$ Due to the environment noise being relatively stable in the adjacent position, δ_σ in all the positions is approximately equal. The following equation can be obtained from equation (13):

$$d_\sigma = \frac{\ln 10}{10n} 10^{\varphi_i/10n} \delta_\sigma d_0. \tag{16}$$

It can be seen from (16) that the distance vector error is exponentially correlated to the signal power attenuation. In order to reduce the distance vector error, a direct mapping between distance and signal power strength should be avoided. Therefore, according to the characteristic of the same environmental factors in the same positions, a difference method is applied (first order) to reduce the multipath effect and, consequently, reduce the environmental noise interference.

Outdoor positioning studies have widely adopted differential positioning technologies. These positioning approaches rely on computations involving two measured values. The values can be collected using two targets and one measuring station, one target and two measuring stations, or one target (measured twice) and one measuring station. With two measured values, the common data items can be removed, which reduces common parameters and errors. Here, we adopt the concept of the outdoor differential positioning method and apply it to our indoor environment. As shown in Figure 8, a schematic for a simple indoor, wireless network system consists of a transmitter (T_1) and two receivers (R_1 and R_2). The distances between the transmitter and the receivers are d_1 and d_2, respectively; d is the distance between the two receivers.

The "free space" electromagnetic wave propagation model is the most basic available. Here, electromagnetic waves emanate along straight lines from a signal source; a spherical space is filled. As shown in Figure 9, according to the Huygens–Fresnel principle, each point on the wave front is a wave source (S) for the secondary radiation of the spherical wave during the transmission of the signal. This wave source is called the secondary wave source. The radiation field at any point in the space is the result of the interference of the waves emitted by the secondary wave

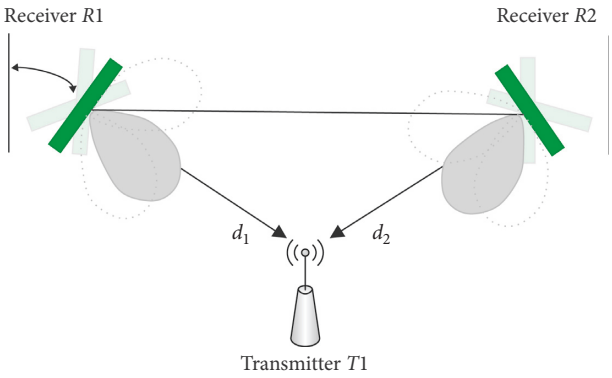

Figure 8: Schematic of multiple receivers of wireless signals.

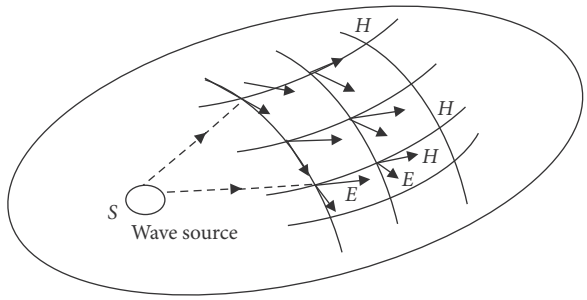

Figure 9: Wireless signal propagation diagram of the Huygens–Fresnel principle.

sources (E, H) at any point on any closed curved surface that surrounds the wave surface. Because the secondary wave source at each point on the closed surface reaches the receiving point differently, the magnitude of the signal field strength at the receiving point changes.

Under normal circumstances with no electromagnetic interference, the propagation of wireless signals in the room conforms to the indoor general attenuation model. This model is a general model under the conditions of a signal source and can be used in a typical indoor environment. The environmental path loss information is characterized by the average path loss and the associated shadow attenuation statistics to characterize the loss of the indoor path. The signal strength received by R_1 and R_2 can be computed using the indoor wireless signal attenuation model:

$$\Pr(d_1) = \Pr(d_0) - 10n\log 10\frac{d_1}{d_0} - X_{\sigma 1}, \tag{17}$$

$$\Pr(d_2) = \Pr(d_0) - 10n\log 10\frac{d_2}{d_0} - X_{\sigma 2}. \tag{18}$$

A first-order differential method is used to eliminate the multipath effect error. Combining (17) with (18) results in

$$\Pr(d_2) - \Pr(d_1) = 10n\log\frac{d_1}{d_2} + X_{\sigma 2} - X_{\sigma 1}. \tag{19}$$

When receivers are in close proximity (i.e., under the small-scale condition), they can be considered to share the same environmental conditions, including the level of multipath effect interference they receive. Hence, when R_1 and R_2 become closer, the interference related to the multipath effect interference is very similar. This similarity allows for the elimination of normal distribution parameters that are common in both receivers:

$$\Pr(d_2) - \Pr(d_1) = 10n\log\frac{d_1}{d_2}. \tag{20}$$

From (20), we can obtain the ratio of d_1 and d_2:

$$\frac{d_2}{d_1} = 10^{(P(d1)-P(d2))/10n}. \tag{21}$$

The power strength of signals collected by receivers is in accordance with (21). Under small-scale conditions, the environmental factor is a constant value for these receivers. Consequently, a differential method can be used to eliminate the common parameters, which avoids the multipath error.

5. The Proposed Differential Positioning Algorithm: Design and Implementation

5.1. Algorithm Design. As shown above, one of the most important things in RFID-based indoor positioning is eliminating noise from receiving signals. And the noise comes from multipath effect of signals. Obviously, the electromagnetic environment indoors is more complex than that outdoors. However, the objects indoors are in the same complex electromagnetic environment. We analysed the loss of path and proposed a method to eliminate the noise.

The deploying of RFID devices is as shown in Figure 10. The RFID tag is stuck to the target, such as book and clothes. And the RFID antennas are installed in the same room with tag. Controlled by the RFID reader, the antennas receive the RFID tag ID as well as the RSSI. When the target is moving in the room, we do not know the position of the target, while the antennas are in a fixed known position.

As shown in Figure 10, there are two antennas and one tag in a room, and the antenna A receives the RSSI value Rssi_A of tag P which is different from the RSSI value received by the antenna B for the reason of different path loss.

The algorithm design draws upon plane geometric and difference localization methods. Beginning with the fundamentals of the plane geometric method, we consider several points on a plane, as shown in Figure 11.

We first consider a simple model. Let point P be the target tag and A and B be antennas. The position of P is $P(x, y)$, and the position of A and B is $(-t, 0)$ and $(t, 0)$, respectively. The X-axis is set using the segment AB; the central perpendicular of AB is set as the Y-axis. According to equation (20), assume that point $P(x, y)$ on the plane satisfies $PA/PB = \lambda$.

It can be obtained from the planar Euclidean distance formula that

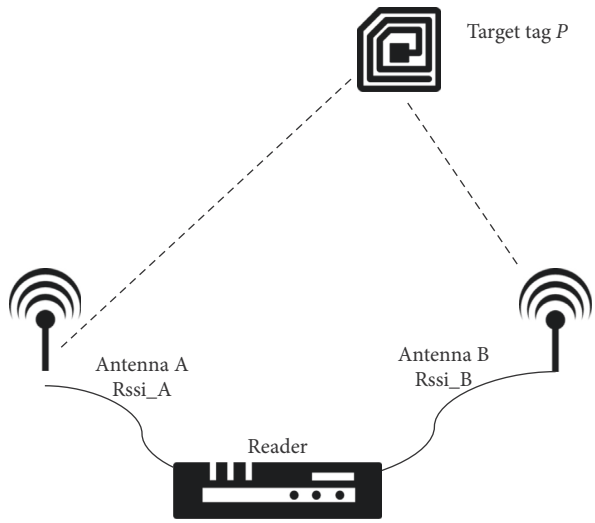

Figure 10: Scenario of RFID applications.

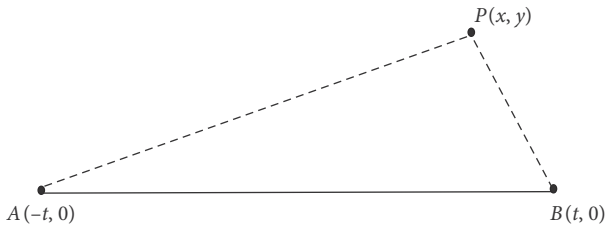

Figure 11: Schematic of distance ratio.

$$\lambda = \frac{PA}{PB} = \sqrt[2]{\frac{(x+t)^2 + y^2}{(x-t)^2 + y^2}}$$

$$\Longrightarrow \lambda^2 = \frac{(x+t)^2 + y^2}{(x-t)^2 + y^2}$$

$$\Longrightarrow \lambda^2\left[(x-t)^2 + y^2\right] = (x+t)^2 + y^2$$

$$\Longrightarrow \lambda^2\left[(x-t)^2 + y^2\right] = (x-t)^2 + y^2 + 4tx$$

$$\Longrightarrow \left(\lambda^2 - 1\right)\left(x^2 - 2tx + t^2\right) + \left(\lambda^2 - 1\right)y^2 - 4tx = 0. \tag{22}$$

When $\lambda \neq 1$, the simplified formula, a circle trajectory equation, is

$$x^2 - 2tx + t^2 + y^2 - \frac{4t}{\lambda^2 - 1}x = 0. \tag{23}$$

As illustrated in Figure 11, $P(x, y)$ satisfies equation (23), where r is the radius of the circle.

$$x^2 - 2t\left(\frac{\lambda^2 + 1}{\lambda^2 - 1}\right)x + t^2 + y^2 = 0. \tag{24}$$

From equation (24), we can get that the track of $P(x, y)$ is a circle:

$$\left(x - \frac{\lambda^2 + 1}{\lambda^2 - 1}t\right)^2 + y^2 = \frac{\lambda^2 t^2\left(\lambda^2 + 2\right)}{\left(\lambda^2 - 1\right)^2}. \tag{25}$$

Let $r^2 = (\lambda^2 t^2(\lambda^2 + 2))/(\lambda^2 - 1)^2$, we can get that

$$\left(x - \frac{\lambda^2 + 1}{\lambda^2 - 1}t\right)^2 + y^2 = r^2. \tag{26}$$

The trajectory of point P satisfies the circle trajectory equation, as shown in Figure 12.

The position $O\ (((\lambda^2 + 1)/(\lambda^2 - 1))t, 0)$ defines the center of the trajectory circle. The trajectory equation defines the line segment AB to have an inner point M and an outer point N; AB is divided according to λ, a constant ratio. The diameter of the trajectory circle is the segment MN. The length of MN can be obtained using the following equations:

$$\begin{cases} \dfrac{d_{AM}}{d_{BM}} = \lambda, \\ \\ d_{AM} + d_{BM} = d_{AB}, \end{cases} \tag{27}$$

$$\begin{cases} \dfrac{d_{AN}}{d_{BN}} = \lambda, \\ \\ d_{AN} + d_{BN} = d_{AB}. \end{cases} \tag{28}$$

The radius of the circle trajectory half of the diameter MN is

$$r = \frac{d_{MN}}{2} = \left|\frac{\lambda}{\lambda^2 - 1}\right| d_{AB}. \tag{29}$$

According to equations (20) and (21), we can find that λ can be calculated using power of the receiving signal, i.e., the RSSI value. And if we choose more than 3 points to receive the signal, the point P would be on the intersection of two circles, as shown in Figure 13.

However, we assume that all points except P are in the X-axis which may not suit the real scenario.

We then considered a more complex model. As shown in Figure 14, let $P(x, y)$ be the target tag, point A, point B, and point C be the antennas controlled by the RFID reader, and their positions be $A(x_A, y_A)$, $B(x_B, y_B)$, and $C(x_C, y_C)$, respectively. Points A, B, and C are chosen without any constraints. Let d_{AB} be the distance of point A and point B and d_{AC} be the distance of point A and point C. Obviously, d_{AB} and d_{AC} are known.

Let $\lambda_1 = PA/PB$ and $\lambda_2 = PC/PB$.

Consider the circle O_1 derived from points P, A, and B such that

$$\lambda_1 = 10^{(\mathrm{RSSI}_B - \mathrm{RSSI}_A)/10n} = \frac{PA}{PB} = \sqrt[2]{\frac{(x - x_A)^2 + (y - y_B)^2}{(x - x_B)^2 + (y - y_B)^2}}. \tag{30}$$

So,

$$\begin{aligned}
\lambda_1^2 &= \frac{(x-x_A)^2+(y-y_A)^2}{(x-x_B)^2+(y-y_B)^2} \\
&\Longrightarrow \lambda_1^2\left[(x-x_B)^2+(y-y_B)^2\right] = (x-x_A)^2+(y-y_A)^2 \\
&\Longrightarrow \lambda_1^2\left[x^2-2x_Bx+x_B^2+y^2-2y_By+y_B^2\right] = x^2-2x_A\cdot x+x_A^2+y^2-2y_Ay+y_A^2 \\
&\Longrightarrow \lambda_1^2x^2-2\lambda_1^2\cdot x_Bx+\lambda_1^2x_B^2+\lambda_1^2y^2-2\lambda_1^2y_By+\lambda_1^2y_B^2-x^2+2x_Ax-x_A^2-y^2+2y_Ay-y_A^2=0 \\
&\Longrightarrow \left(\lambda_1^2-1\right)x^2-2\cdot\left(\lambda_1^2x_B-x_A\right)\cdot x+\left(\lambda_1^2-1\right)y^2-2\left(\lambda_1^2y_B-y_A\right)y+\lambda_1^2x_B^2+\lambda_1^2y_B^2-x_A^2-y_A^2=0.
\end{aligned} \tag{31}$$

If $\lambda_1^2 \neq 1$, then

$$\begin{aligned}
&x^2-2\left(\frac{\lambda_1^2x_B-x_A}{\lambda_1^2-1}\right)x+y^2-2\left(\frac{\lambda_1^2\cdot y_B-y_A}{\lambda_1^2-1}\right)y+\frac{\lambda_1^2\left(x_B^2+y_B^2\right)-\left(x_A^2+y_A^2\right)}{\lambda_1^2-1}=0, \\
&\cdot\left(x-\frac{\lambda_1^2x_B-x_A}{\lambda_1^2-1}\right)^2+\left(y-\left(\frac{\lambda_1^2\cdot y_B-y_A}{\lambda_1^2-1}\right)\right)^2 \\
&=\left(\frac{\lambda_1^2x_B-x_A}{\lambda_1^2-1}\right)^2+\left(\frac{\lambda_1^2y_B-y_A}{\lambda_1^2-1}\right)^2-\frac{\lambda_1^2\left(x_B^2+y_B^2\right)-\left(x_A^2+y_A^2\right)}{\lambda_1^2-1} \\
&=\frac{\left(\lambda_1^4x_B^2-x_A\right)^2+\left(\lambda_1^2y_B-y_A\right)^2-\left(\lambda_1^2-1\right)\left[\lambda_1^2\left(x_B^2+y_B^2\right)-\left(x_A^2+y_A^2\right)\right]}{\left(\lambda_1^2-1\right)^2} \\
&=\frac{\lambda_1^4x_B^2-2\lambda_1^2x_Ax_B+x_A^2+\lambda_1^4y_B^2-2\lambda_1^2\cdot y_A\cdot y_B+y_A^2}{\left(\lambda_1^2-1\right)^2}-\frac{-\left[\lambda_1^4\left(x_B^2+y_B^2\right)-\lambda_1^2\left(x_A^2+y_A^2\right)-\lambda_1^2\left(x_B^2+y_B^2\right)+x_A^2+y_A^2\right]}{\left(\lambda_1^2-1\right)^2} \\
&=\frac{\lambda_1^4\left(x_A^2+y_B^2\right)-2\lambda_1^2\left(x_A\cdot x_B+y_A-y_B\right)+\left(x_A^2+y_A^2\right)-\lambda_1^4\left(x_B^2+y_B^2\right)}{\left(\lambda_1^2-1\right)^2}+\frac{\lambda_1^2\left(x_A^2+y_A^2\right)+\lambda_1^2\left(x_B^2+y_B^2\right)-\left(x_A^2+y_A^2\right)}{\left(\lambda_1^2-1\right)^2} \\
&=\frac{\lambda_1^2\left(x_A^2+y_A^2+x_B^2+y_B^2-2x_A\cdot x_B-2y_A\cdot y_B\right)}{\left(\lambda_1^2-1\right)^2} \\
&=\frac{\lambda_1^2}{\left(\lambda_1^2-1\right)^2}\left[(x_A-x_B)^2+(y_A-y_B)^2\right]=\frac{\lambda_1^2}{\left(\lambda_1^2-1\right)^2}\cdot d_{AB}^2.
\end{aligned} \tag{32}$$

We get the circle derived from points P, A, and B:

$$\left(x-\frac{\lambda_1^2\cdot x_B-x_A}{\lambda_1^2-1}\right)^2+\left(y-\frac{\lambda_1^2\cdot y_B-y_A}{\lambda_1^2-1}\right)^2=\frac{\lambda_1^2}{\left(\lambda_1^2-1\right)^2}\cdot d_{AB}^2. \tag{33}$$

The center of the circle is $O_1((\lambda_1^2x_B-x_A/\lambda_1^2-1),(\lambda_1^2\cdot y_B-y_A/\lambda_1^2-1))$.

The radius $r_1=|\lambda_1/\lambda_1^2-1|\cdot d_{AB}$.

And we can get another circle derived from points P, A, and C:

$$\left(x-\frac{\lambda_2^2\cdot x_C-x_A}{\lambda_2^2-1}\right)^2+\left(y-\frac{\lambda_2^2\cdot y_C-y_A}{\lambda_2^2-1}\right)^2=\frac{\lambda_2^2}{\left(\lambda_2^2-1\right)^2}\cdot d_{AC}^2. \tag{34}$$

The center of the circle is $O_2((\lambda_2^2x_C-x_A/\lambda_2^2-1),(\lambda_2^2\cdot y_C-y_A/\lambda_2^2-1))$.

The radius $r_2=|\lambda_2/\lambda_2^2-1|\cdot d_{AC}$.

According to equations (33) and (34), the intersection points can be solved, which are point P.

About λ_1, if $\lambda_1 = \pm 1$, point P is on the mid-vertical line of AB connection.

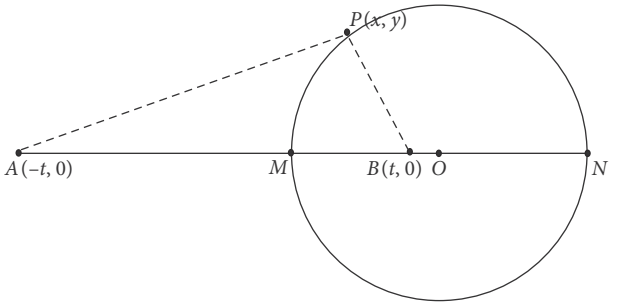

Figure 12: Schematic of the circle trajectory for a moving target.

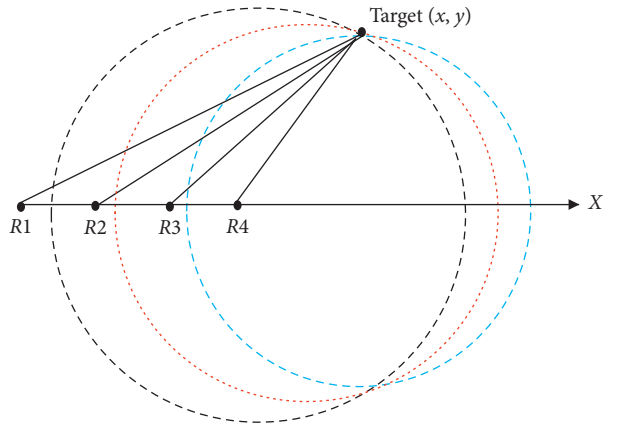

Figure 13: Schematic of multiple receivers with intersecting circular trajectories (target positioning).

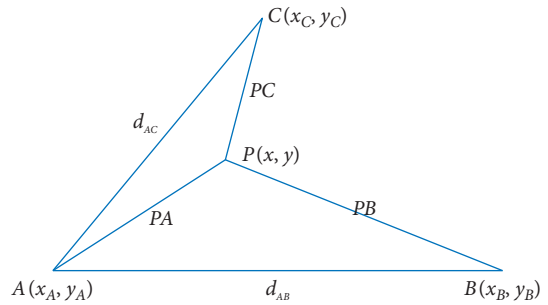

Figure 14: Position of 3 receiving points and 1 target point.

In summary, simultaneously from all the circles' equation or lines' equation, we can get the target point P.

5.2. Algorithm Implementation

5.2.1. Movement Signal Receiver Matrix. In order to obtain the overlapped domain of multiple circle trajectories, multiple signal receivers should be set to collect power strength measurements. Considering the cost and difficulty of deployment, we apply the movement signal receiver method to extend the receiving range of a single signal receiver. This method can result in a reduction in the deployment density of receivers and algorithm cost. As shown in Figure 15, based on the relative movement principle, we

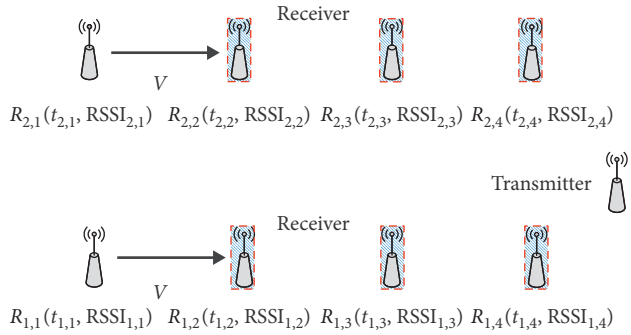

Figure 15: Schematic of the generation of virtual receivers.

make the wireless signal receiver move in a fixed direction [33, 34].

The displacement of the signal receiver can be described in the following equation, where $D(t)$ is the displacement of the receiver R at the timepoint t and t_0 is the initial timepoint:

$$D(t) = D(t_0) + \int_{t_0}^{t} \overrightarrow{V}(t)\mathrm{d}t. \tag{35}$$

Knowing the initial position of the receiver and migration velocity, we can calculate the displacement of the receiver R at different times using the following equation:

$$d_{R_i R_{i+1}} = D(t_{i+1}) - D(t_i). \tag{36}$$

Thus, the coordinates of M receivers $R_1, \ldots, R_M$ at different timepoints can be determined. The displacements of M moving receivers can be presented by the matrix, which is composed of receivers' moving positions at N different timepoints:

$$\begin{pmatrix} R_{1,1} & \cdots & R_{1,N} \\ \vdots & \vdots & \vdots \\ R_{M,1} & \cdots & R_{M,N} \end{pmatrix}. \tag{37}$$

5.2.2. Data Acquisition and Pretreatment. Using the migration receiver matrix to collect the power strength of wireless signals can obtain the signal power strength of different positions, which can effectively reduce the hardware deployment cost and improve the equipment utilization in the premise of ensuring data acquisition quality.

We organize the data in a standardized quadruple: time, strength value, ID, and displacement:

$$R_{i,j} = \text{<TimeStamp, RSSI, ID, Position>}. \tag{38}$$

Aiming at the wireless signal noise and errors in the time domain of the receivers at the same position, a smoothing treatment has been done by the designed single exponential smoothing method in order to reduce the time-domain error. The formula is as follows:

$$\mathrm{RSSI}_t = \alpha \sum_{n=0}^{t} (1-\alpha)^n \mathrm{RSSI}_{\{t-n\}}. \quad (39)$$

By using the single exponential smoothing method for the signal strength of adjacent nodes in the moving receiver matrix, the signal strength deviation caused by noises can be reduced. At this step, the distance ratio in the following equation can be calculated to obtain the circular trajectory of the target:

$$\lambda = 10^{\left(R_{i,j}(\mathrm{RSSI}) - R_{i,j+1}(\mathrm{RSSI})\right)/10n}. \quad (40)$$

5.2.3. Heuristic Alternative for Determining a Target Position. As indicated in Section 5.1, one approach to determining a target's position is to establish and solve a system of circular trajectory equations for the intersection coordinates. However, this is a computationally expensive problem that also relies on the difficult task of sensor deployment in real applications. To reduce the calculation complexity, a Monte Carlo simulation is adopted. The target position's coordinates are obtained using a fuzzy map-based strategy. The plane is divided into square units (10 cm ∗10 cm) establishing a Cartesian coordinate system (refer to Figure 16) [35].

Each unit area is assessed on whether or not it falls within the generated target circular trajectory; the coordinates of the target circular trajectory are (X_{oi}, Y_{oi}).

$$d_i = \sqrt{\left\{(X_i - X_{oi})^2 + (Y_i - Y_{oi})^2\right\}} \le R_i. \quad (41)$$

Each area is marked as either 0 (it is not within the trajectory) or 1 (it is within the trajectory). In the following equation, R_i is the radius of the i-th circle in (34):

$$T_i = \begin{cases} 0, & \text{when } d_i > R_i, \\ 1, & \text{when } d_i \le R_i. \end{cases} \quad (42)$$

This assessment is conducted for each movement of a receiver.

Next, the unit areas within a circular trajectory, marked as 1, are viewed as a fuzzy map. A fuzzy map is generated to represent each movement of a receiver during one cycle.

Hence, the intersection total for each unit area can be counted over a collection of fuzzy maps (k represents the number of receiver movements) as

$$Sk(T_i) = \sum_{i=1}^{n} T_i. \quad (43)$$

Once these are counted, heat map can be generated to visualize the results (refer to Figure 17). Here, the area with a higher possibility of containing the target position has a deeper color.

Going beyond a visual inspection, the fuzzy maps can be used to compute the most likely position of the target by solving the intersection coordinates. When solving for the target coordinate, two weights are considered.

The first weight, W_{1i}, reflects the overall, containing density of the number of unit areas (T_i) that fall within a

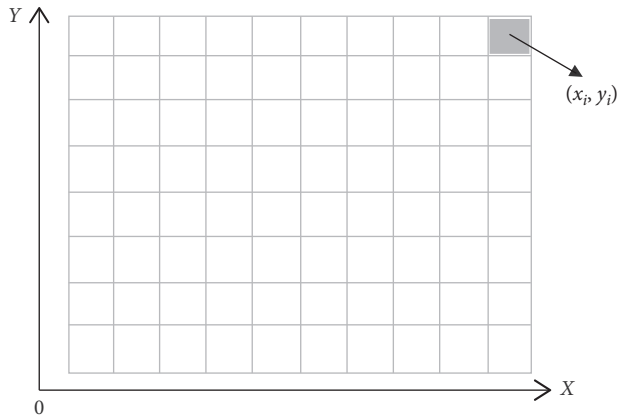

Figure 16: Indoor plane: establishing Cartesian coordinates.

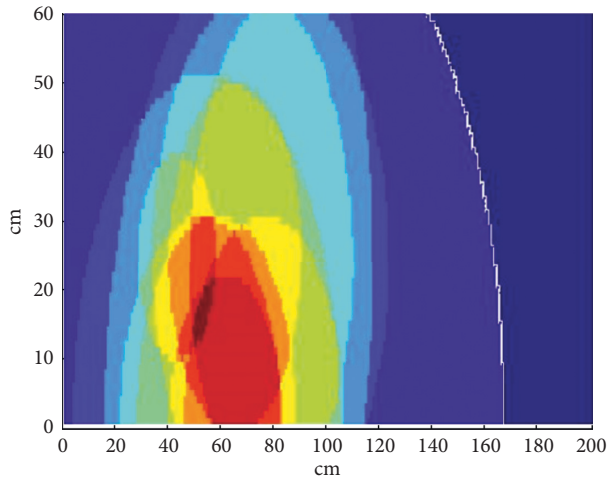

Figure 17: Schematic of a heat map visualization.

circular trajectory over all of the movement cycles (K) represented in maps (refer to equation (44)). A higher number of unit areas contained within a trajectory result in a higher density and W_{1i}:

$$W_{1i} = \frac{\sum_{k=1}^{k} S_k(T_i)}{\sum_{k=1}^{k}\sum_{i=1}^{n} S_k(T_i)}. \quad (44)$$

The second weight, W_{2i}, reflects the density of one particular unit area, T_i (refer to equation (45)). Here, n_{ci} is the number of the candidate unit areas connected with the candidate unit area being considered, T_i. The number of candidate unit areas selected from the complete positioning domain is n_a. When the density of the candidate unit area connected with ci is larger, the weight W_{2i} is also larger:

$$W_{2i} = \frac{n_{ci}}{\sum_{i=1}^{n_a} n_{ci}}. \quad (45)$$

Using the total weight, W_i is the product of W_{1i} and W_{2i}:

$$W_i = W_{1i} \times W_{2i}. \quad (46)$$

Using the calculated total weights, the target location can be calculated using

$$(x, y) = \sum_{i=1}^{n_a} W_{i(x_i, y_i)}. \quad (47)$$

6. Algorithm Test and Result Analysis

6.1. Testing Environment and Equipment. As shown in Figure 18, two test spaces are designed in the laboratory. The first space has little environmental interference, whereas the second space has substantial environmental interference. Both of the spaces exceed 150 m^2. Within each space, the target is randomly positioned. The test system moves the wireless receiver along the guide rail (fixed speed) and collects the signal data parameters. The environment factors are set to 1.8 based on experience.

The laboratory space and test equipment utilized in the empirical studies are summarized in this section. The wireless hardware includes Bluetooth and RFID equipment. For Bluetooth testing, the NORDIC nRF51422 processor chip and the Arduino open-source hardware platform are used. For RFID testing, the Impinj R420 (Figure 19) device is used.

As shown in Figure 20, we attached the signal receiver to the motor guide rail. The testing system moved the receiver along the guide rail. The speed is fixed; the testing system pauses this movement once a second to receive the signal.

During the actual operation of the algorithm, the asynchrony of data acquisition at the sensing layer and the time delay of data transmission at the network layer cause the integrity of the standard four-tuple data acquired by the application layer to be not guaranteed. Therefore, integrity checking rules need to be applied at the application layer to ensure that the positioning algorithm calculates the correct result. The steps to apply these rules are as follows: First, the application layers retrieve the data from the message middleware layer and populate an array, with L rows and four columns. Each row stores a signal sample acquired by the reader; the four columns store the standardized quadruple of data, $R_{i,j}$. The two-dimensional array is shown in Figure 21. The RSSI values are in the range $[-90, 0]$.

The system encapsulates the two-dimensional array matrix arranged at each moment into a data packet and performs integrity detection on the two-dimensional array in the generated data packet before calculating the positioning. If the data in the matrix are complete, the difference geometry positioning is performed. If the data in the matrix are incomplete, the data packet is discarded to ensure the reliability s of the indoor positioning algorithm's output. According to the steps of the differential geometric positioning algorithm, the distance ratio is calculated by the RSSI difference of the target tag when the reader moves at different positions, and the actual position of the tag to be measured is obtained according to the fuzzy map calculation method.

Since the actual data collection rate of position location technologies (e.g., RFID) is at a very high level, it is necessary to use a sliding window in the message middleware layer to organize the collected data packets for efficient processing. The test system sets 0.5 s as the data collection interval. Within one window, only the data packets with the first time stamp are initially considered; if these data are complete, the algorithm calculation is performed. Otherwise, the first set of data is discarded and the second set of data in the entire time window is considered.

6.2. Experimental Design and Discussion of the Results

6.2.1. Designing the Laboratory Test Spaces

(1) Small test area: as shown in Figure 18, there is a small test area. It is a narrow corridor full of debris and a typical indoor environment full of noise signals. The area is 4.8 m in length, 3.5 m in width, and 3 m in height. In the area, we test the RFID-based indoor positioning method we proposed to measure the accuracy of the method.

(2) Large test area: as shown in Figure 22, we simulated two scenarios in the same space in the laboratory. The area is 8 m in length, 7 m in width, and 3 m in height. We chose the area for the purpose of simulating the warehouse that is full of shelves to put something such as books, pharmaceutical supplies, and mechanical components. The positioning strategy can be effectively applied to the aforementioned or similar scenarios. Using the guide rail instead of multiple RFID readers in a scene has the following advantages: (1) The result of using guide rail measurement is robust. The result of continuous measurement has better accuracy than that of discrete measurement after smoothing. (2) The guide rail can effectively save space. In the actual scene, multiple RFID readers may be difficult to deploy and distributed readers may bring further complex processing in collaboration. (3) In addition to space savings, the cost of a single guide rail is lower than that of multiple RFID readers economically. Therefore, the following experiments can be used to simulate the actual large-scale scene.

Figure 22(a) simulates the scenario which has no obstacle in the space. And in Figure 22(b), we put some high plants to simulate the scenario which has some obstacles in the space. Both of the spaces exceed 150 m^2. Within each space, the target is randomly positioned. The test system moves the wireless receiver along the guide rail (fixed speed) and collects the signal data parameters. The environment factors are set to 1.8 based on experience.

For measuring the accuracy of the algorithm, the RMSE is computed using the following equation (48), where (x, y) are the real coordinates of the target and (x_1, y_1) are the computed results using the proposed algorithm:

$$\text{RMSE} = E\left[(x - x_1)^2 + (y - y_1)^2\right]^{1/2}. \quad (48)$$

Figure 18: Small test area.

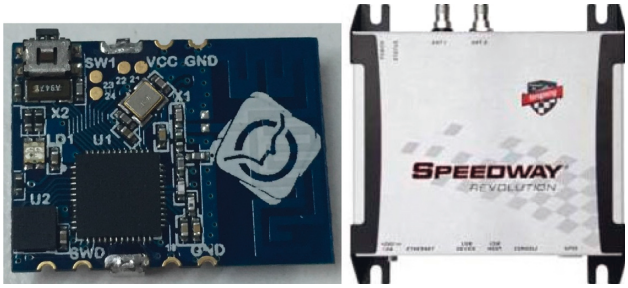

Figure 19: Bluetooth and RFID test devices.

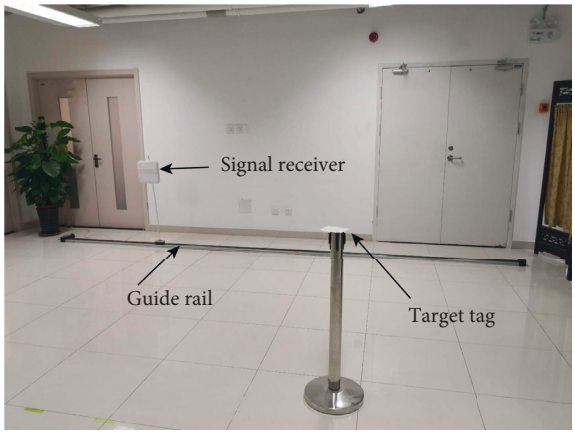

Figure 20: Motor guide rail and the signal receiver.

$$M = \begin{bmatrix} \text{Timestamp}_1 & \text{IPAddress}_1 & \text{Tag}ID_2 & \text{RSSI}_1 \\ \text{Timestamp}_1 & \text{IPAddress}_1 & \text{Tag}ID_3 & \text{RSSI}_2 \\ \text{Timestamp}_1 & \text{IPAddress}_1 & \text{Tag}ID_1 & \text{RSSI}_3 \\ \text{Timestamp}_1 & \text{IPAddress}_1 & \text{Tag}ID_4 & \text{RSSI}_4 \\ \text{Timestamp}_1 & \text{IPAddress}_1 & \text{Tag}ID_5 & \text{RSSI}_5 \\ \text{Timestamp}_1 & \text{IPAddress}_2 & \text{Tag}ID_3 & \text{RSSI}_6 \\ \text{Timestamp}_1 & \text{IPAddress}_2 & \text{Tag}ID_5 & \text{RSSI}_7 \\ \text{Timestamp}_1 & \text{IPAddress}_2 & \text{Tag}ID_2 & \text{RSSI}_8 \\ \text{Timestamp}_1 & \text{IPAddress}_2 & \text{Tag}ID_1 & \text{RSSI}_9 \\ \text{Timestamp}_1 & \text{IPAddress}_2 & \text{Tag}ID_1 & \text{RSSI}_{10} \\ \text{Timestamp}_1 & \text{IPAddress}_3 & \text{Tag}ID_5 & \text{RSSI}_{11} \\ \text{Timestamp}_1 & \text{IPAddress}_3 & \text{Tag}ID_2 & \text{RSSI}_{12} \\ \text{Timestamp}_1 & \text{IPAddress}_3 & \text{Tag}ID_3 & \text{RSSI}_{13} \\ \text{Timestamp}_1 & \text{IPAddress}_3 & \text{Tag}ID_4 & \text{RSSI}_{14} \\ \text{Timestamp}_1 & \text{IPAddress}_3 & \text{Tag}ID_1 & \text{RSSI}_{15} \end{bmatrix}$$

Figure 21: Organization of the two-dimensional array (application layer).

6.2.2. Assessing the Accuracy of the Proposed Algorithm

(1) Small area test: the experiments in this area are used to verify the accuracy and feasibility of the algorithm. As shown in Figure 18, we deployed four antennas in the corridor, placed an RFID tag in the area, and used one reader to receive the RFID signal. The received signal is shown in Figure 23, where the same antenna continuously receives multiple data. Because the tag is static in the area, we assume that the first data are the earliest one among the data received by each antenna continuously. Then, according to the time sequence, the tag position is processed and calculated according to the previous method.

After getting the tag position, the deviation between the calculated value and the actual position is shown in Figure 24, and the RMSE is 0.20. The test results show that the proposed indoor location algorithm is effective and has high accuracy in static tags.

(2) Large area test: to evaluate the accuracy of our algorithm, we collect data from 30 experimental runs

(a) (b)

Figure 22: Large test area. (a) Laboratory space for test 1. (b) Laboratory space for test 2.

EPC	RSSI	Antenna number	Time
EPC1	−46	2	Time1
~~EPC1~~	~~−45.5~~	~~2~~	~~Time1~~
EPC1	−60.5	3	Time1
~~EPC1~~	~~−61.5~~	~~3~~	~~Time1~~
EPC1	−66	1	Time1
~~EPC1~~	~~−62.5~~	~~1~~	~~Time1~~
EPC1	−46	2	Time1
EPC1	−46	2	Time1
EPC1	−60.5	3	Time1
EPC1	−60.5	3	Time1
EPC1	−52	4	Time1
EPC1	−51.5	4	Time1
EPC1	−66	1	Time1
EPC1	−64	1	Time1
EPC1	−45.5	2	Time1
EPC1	−46	2	Time1
EPC1	−61	3	Time1
EPC1	−61	3	Time1
EPC1	−51.5	4	Time1
EPC1	−51.5	4	Time1
EPC1	−66	1	Time1
EPC1	−66	1	Time1
EPC1	−46	2	Time1

Figure 23: Data preprocessing.

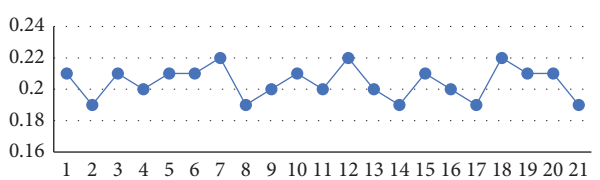

Figure 24: Distance deviation between the calculated value and the real value in a small area.

for both tests 1 and 2, using both Bluetooth and RFID technologies (120 runs in total). The RMSE is computed to assess the accuracy. The results are illustrated in Figure 25.

Table 2 presents a summary of the experimental results. The average error in our experiments ranges from 46 to 62 cm, achieving approximately 55 cm overall, spanning the two distinct test spaces and position location technologies. Its accuracy is better in the environment with little interference (test 1), which is to be expected. Examining the average error results in the environment with substantial interference (test 2), the algorithm performs quite well. In addition, the variance results are quite low which indicates the algorithm is stable.

6.2.3. Comparing the Accuracy of the Proposed Algorithm. The accuracy of the proposed algorithm is further assessed in a comparative experiment involving two existing approaches: the LANDMARC and trilateration positioning algorithms. In this experiment, the test 2 area (substantial environmental interference) is used; we collect data from 30 experimental runs, using RFID and Bluetooth devices and all three algorithms (180 runs in total). Figure 26 illustrates the results using the RFID technology, and Figure 27 presents the results using Bluetooth.

The experimental results using the RFID technology are summarized in Table 3, and Table 4 presents the results using the Bluetooth technology.

The results indicate the proposed algorithm is more accurate than the trilateration positioning and LANDMARC positioning approaches in the test area with substantial environmental interference. The proposed algorithm achieves an average RMSE that is less than 0.65 m in the indoor environment. Comparatively, the error of the proposed approach is much lower than that of both the trilateration positioning algorithm (approximately 20% its error) and the LANDMARC positioning algorithm (approximately 30% of its error). In addition, the comparison of the variance results indicates the proposed algorithm also offers better stability than the other two approaches in this study.

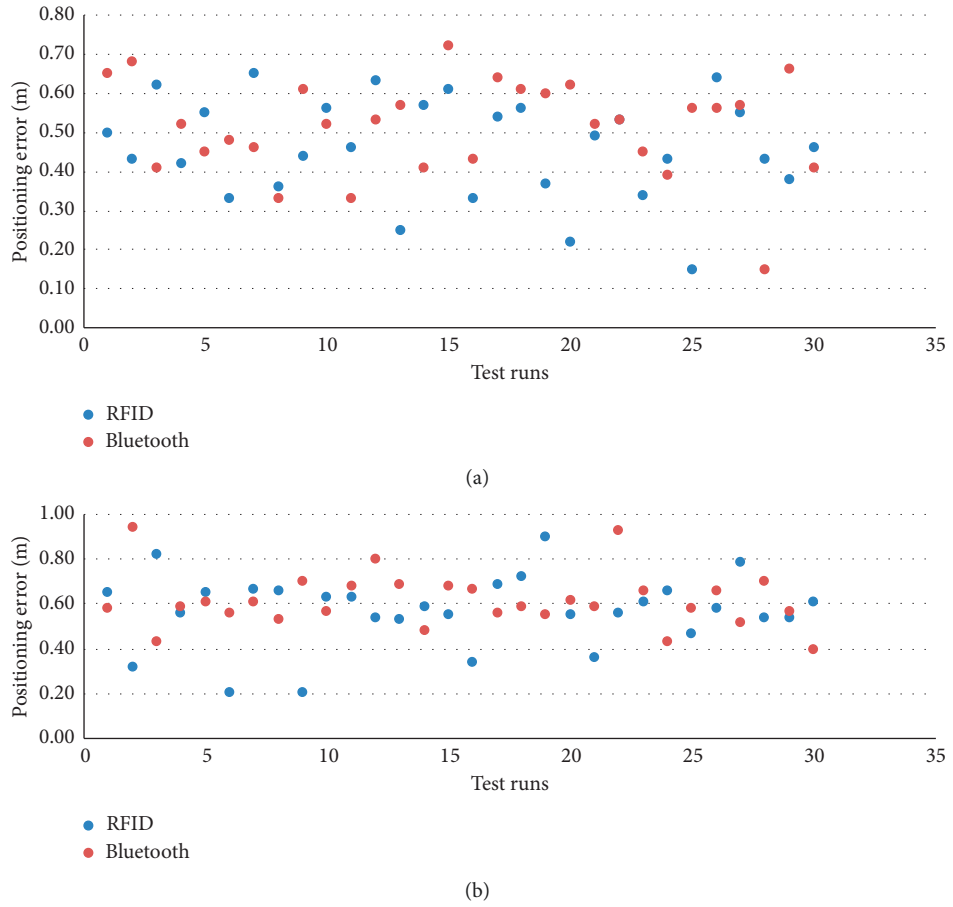

Figure 25: Positioning algorithm's RMSE results. (a) Positioning error results in test area 1 (little environmental interference). (b) Positioning error results in test area 2 (substantial environmental interference).

Table 2: Experimental results: RMSE summary statistics.

Device technology	Test area	Min. error	Max. error	Average error	Variance
RFID	Area 1	0.15	0.65	0.46	0.13
RFID	Area 2	0.21	0.90	0.57	0.16
Bluetooth	Area 1	0.15	0.72	0.51	0.12
Bluetooth	Area 2	0.40	0.94	0.62	0.12

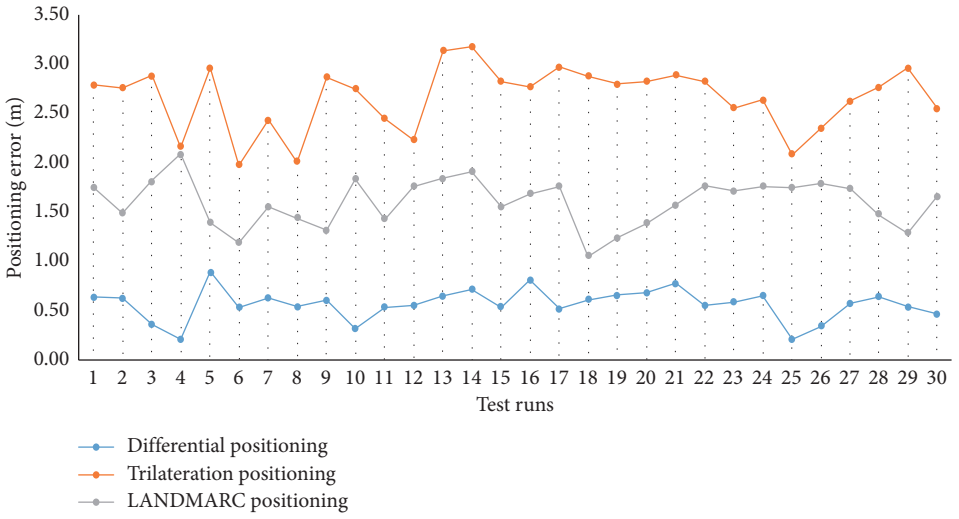

Figure 26: Positioning algorithms' error comparative results (RFID technology).

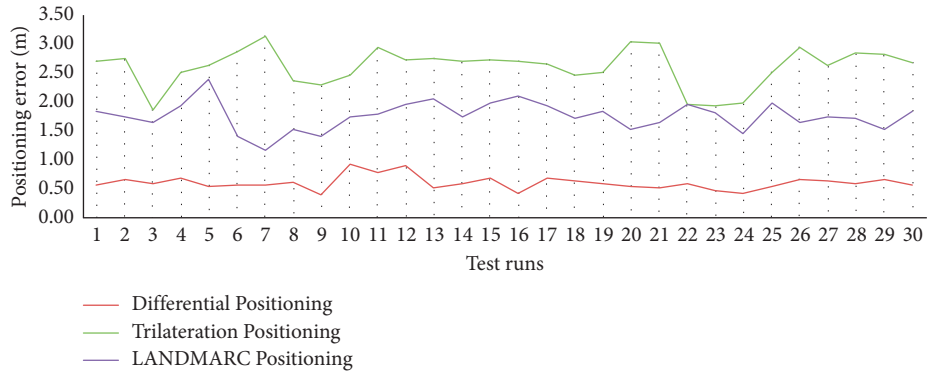

Figure 27: Positioning algorithms' error comparative results (Bluetooth technology).

Table 3: Comparative experimental results: RMSE summary statistics (RFID technology).

Algorithm	Min. error	Max. error	Average error	Variance
Differential positioning	0.21	0.90	0.57	0.16
Trilateration positioning	1.98	3.19	2.67	0.32
LANDMARC positioning	1.05	2.10	1.61	0.24

Table 4: Comparative experimental results: RMSE summary statistics (Bluetooth technology).

Algorithm	Min. error	Max. error	Average error	Variance
Differential positioning	0.40	0.94	0.62	0.12
Trilateration positioning	1.90	3.20	2.65	0.33
LANDMARC positioning	1.19	2.43	1.79	0.25

7. Conclusion and Future Work

A novel positioning algorithm is proposed in this work for use in indoor environments with wireless communication. The algorithm is designed using a plane geometric method and difference localization theory. The algorithm is implemented; its accuracy and adaptability to different location position technologies (RFID and Bluetooth) are empirically evaluated in two distinct test environments. Furthermore, in a comparative evaluation involving established trilateration positioning and LANDMARC positioning approaches, the proposed algorithm achieves the best accuracy while also providing stability in the results. The proposed algorithm can also help reduce the deployment cost by adopting the movement antenna matrix method and reducing the number of sensors needed, thus improving its feasibility for use in real-world applications.

There are many interesting directions for the future work. Investigating further improvements to the accuracy of the proposed algorithm is planned. For example, one improvement is to replace the signal strength parameter, RSSI, with a probability parameter. This may be accomplished by using a Gaussian distribution model to compute the probability of a target position. A second direction is to extend the approach and the test system architecture to also support access to geographic data. This extension would support a combination of real geographic data and indoor location positioning capabilities, which may be valuable for developing practical systems.

Data Availability

The data used to support the findings of this study are available from the corresponding author upon request.

Disclosure

This paper is an extended version of a conference paper, which was published at the 12th International Conference on Wireless Algorithms, Systems, and Applications (WASA 2017), named "Design and Realization of an Indoor Positioning Algorithm Based on Differential Positioning Method." The funders had no role in the design of this study; in the collection, analyses, or interpretation of data; in the writing of the manuscript; or in the decision to publish the results.

Conflicts of Interest

The authors declare no conflicts of interest.

Authors' Contributions

Siye Wang and Chang Ding conceived the presented idea, developed the theory, and performed the computations. Chang Ding and Yanfang Zhang conducted the experiment

to verify the idea. Shaoyi Zhu and Yue Cui applied the proposed differential position algorithm to a software program and collected the experiment data from the RFID device and Bluetooth device, respectively. Yanfang Zhang carried out the experiment about the relationship between RSSI and distance. Weiqing Huang and Jianguo Jiang helped supervise the project. Siye Wang and Chang Ding wrote the original draft in consultation with Weiqing Huang and Jianguo Jiang. Junyu Lin contributed to the interpretation of the results. All authors provided critical feedback and helped shape the research, analysis, and manuscript.

Acknowledgments

This research was funded by the National Key Research and Development Project under grant no. 2018YFF0301202.

References

[1] Z. Yang, Y. Liu, and Z. Zhou, "From RSSI to CSI: indoor localization via channel response," *ACM Computing Surveys*, vol. 46, no. 2, pp. 1–32, 2013.

[2] Q. Pu, S. Gupta, S. Gollakota, and P. Patel, "Whole-home gesture recognition using wireless signals (demo)," in *Proceedings of the 19th Annual International Conference on Mobile Computing and Networking*, pp. 27–38, Miami, FL, USA, October 2013.

[3] Y. Wang, J. Liu, Y. Chen, M. Gruteser, J. Yang, and H. Liu, "E-eyes: device-free location-oriented activity identification using fine-grained WiFi signatures," in *Proceedings of the 2014 International Conference on Mobile Computing and Networking*, pp. 617–628, New York, NY, USA, October 2014.

[4] J. Wang, D. Vasisht, and D. Katabi, "RF-IDraw: virtual touch screen in the air using RF signals," *ACM SIGCOMM Computer Communication*, vol. 44, no. 4, pp. 235–246, 2014.

[5] V. Falco, R. Want, A. Hopper, and J. Gibbons, "The active badge location system," *ACM Transactions on Information Systems*, vol. 10, no. 1, pp. 91–102, 1992.

[6] N. B. Priyantha, A. Chakraborty, and H. Balakrishnan, "The cricket location-support system," in *Proceedings of the 2000 International Conference on Mobile Computing and Networking*, pp. 32–43, Boston, MA, USA, August 2000.

[7] N. B. Priyantha, *The Cricket Indoor Location System*, Massachusetts Institute of Technology, Cambridge, MA, USA, 2005.

[8] D. X. Jiang, H. U. Ming-Qing, Y. Q. Chen, J. F. Liu, and J. Y. Zhou, "Adaptive Bluetooth location method based on kernel ridge regression," *Application Research of Computers*, vol. 27, pp. 3487–3486, 2010.

[9] Z. Jie, L. Hong-li, L. Shu-gang, and Z. Fan, "The study of dynamic DegreeWeighted centroid localization algorithm based on RSSI (in Chinese)," *Acta Electronica Sinica*, vol. 39, pp. 82–88, 2011.

[10] H. Zhu, M. Li, I. Chlamtac, and B. Prabhakaran, "Survey of quality of service in IEEE 802.11 networks," *IEEE Wireless Communications*, vol. 11, no. 4, pp. 6–14, 2004.

[11] A. Soomro and D. Cavalcanti, "Opportunities and challenges in using WPAN and WLAN technologies in medical environments (accepted from open call)," *IEEE Communications Magazine*, vol. 45, no. 2, pp. 114–122, 2007.

[12] A. Varshavsky, E. D. Lara, J. Hightower, A. Lamarca, and V. Otsason, "GSM indoor localization," *Pervasive and Mobile Computing*, vol. 3, no. 6, pp. 698–720, 2007.

[13] Y. Shimizu and Y. Sanada, "Accuracy of relative distance measurement with ultra wideband system," in *Proceedings of the IEEE Conference on Ultra Wideband Systems and Technologies*, pp. 374–378, Reston, VA, USA, November 2003.

[14] J. Y. Lee and R. A. Scholtz, "Ranging in a dense multipath environment using an UWB radio link," *IEEE Journal on Selected Areas in Communications*, vol. 20, no. 9, pp. 1677–1683, 2002.

[15] B. Song, L. Cheng, M. Zhou, H. Wu, and Y. Chen, "The design of cellphone indoor positioning system based magnetic assisted inertial navigation technology," *Chinese Journal of Sensors and Actuators*, vol. 28, no. 8, 2015.

[16] W. Xu-feng, *The research on inertial sensor-base indoor localization system*, Ph.D. thesis, Jilin University, Changchun, China, 2015.

[17] J. Hightower, G. Borriello, and R. Want, "SpotON: an indoor 3d location sensing technology based on rf signal strength," CSE report, University of Washington, Seattle, WA, USA, 2000.

[18] G. B. Chris Vakili, "Design and calibration of the spoton Ad-hoc location sensing system," CSE report, University of Washington, Seattle, WA, USA, 2001.

[19] X. Bao and G. Wang, "Random sampling algorithm in RFID indoor location system," in *Proceedings of the IEEE International Workshop on Electronic Design, Test and Applications*, pp. 168–176, Kuala Lumpur, Malaysia, January 2006.

[20] J. Wang and Z. Shen, "An improved music toa estimator for RFID positioning," in *Proceedings of the RADAR 2002*, pp. 478–482, Edinburgh, UK, 2002.

[21] T. F. Bechteler and H. Yenigun, "2D localization and identification based on SAW ID-tags at 2.5 GHz," *IEEE Transactions on Microwave Theory and Techniques*, vol. 51, no. 5, pp. 1584–1590, 2003.

[22] D. D. Arumugam, D. W. Engels, and M. H. Mickle, "Method for the real-time localization of passive SAW-based RFID systems around corners," in *Proceedings of the Military Communications Conference MILCOM 2008*, pp. 1–7, San Diego, CA, USA, November 2008.

[23] L. M. Ni, Y. Liu, Y. C. Lau, and A. P. Patil, "LANDMARC: indoor location sensing using active RFID," *Wireless Networks*, vol. 10, no. 6, pp. 701–710, 2004.

[24] G. Y. Jin, X. Y. Lu, and M. S. Park, "An indoor localization mechanism using active RFID tag," in *Proceedings of the IEEE International Conference on Sensor Networks, Ubiquitous, and Trustworthy Computing -Vol 1 (SUTC'06)*, pp. 40–43, Taichung, Taiwan, June 2006.

[25] A. Chattopadhyay and A. R. Harish, "Analysis of UHF passive RFID tag behavior and study of their applications in low range indoor location tracking," in *Proceedings of the Antennas and Propagation Society International Symposium*, pp. 1217–1220, Honolulu, HI, USA, June 2007.

[26] A. Chattopadhyay and A. R. Harish, "Analysis of low range indoor location tracking techniques using passive UHF RFID tags," in *Proceedings of the 2008 IEEE Radio and Wireless Symposium*, Orlando, FL, USA, January 2008.

[27] J. S. Choi, H. Lee, R. Elmasri, and D. W. Engels, "Localization systems using passive UHF RFID," in *Proceedings of the International Joint Conference on Inc, Ims and IDC*, pp. 1727–1732, Seoul, South Korea, August 2009.

[28] Y. Zhao, Y. Liu, and L. M. Ni, "VIRE: active RFID-based localization using virtual reference elimination," in *Proceedings of the International Conference on Parallel Processing*, p. 56, Xi'an, China, September 2007.

[29] H. Xu, M. Wu, P. Li, F. Zhu, and R. Wang, "An RFID indoor positioning algorithm based on support vector regression," *Sensors*, vol. 18, no. 5, p. 1504, 2018.

[30] H. Xu, D. Ye, P. Li, R. Wang, and Y. Li, "An RFID indoor positioning algorithm based on bayesian probability and K-nearest neighbor," *Sensors*, vol. 17, no. 8, p. 1806, 2017.

[31] J. Werb and C. Lanzl, "Designing a positioning system for finding things and people indoors," *Spectrum IEEE*, vol. 35, no. 9, pp. 71–78, 1998.

[32] H. Zhu, X. Fu, L. Sun, X. Xie, and R. Wang, "CSI-based Wi Fi environment sensing," *Journal of Nanjing University of Posts and Telecommunications*, vol. 36, no. 1, 2016.

[33] Y. Lei, Y. Chen, X. Y. Li, C. Xiao, L. Mo, and Y. Liu, "Tagoram: real-time tracking of mobile RFID tags to high precision using COTS devices," in *Proceedings of the International Conference on Mobile Computing and Networking*, Maui, HI, USA, September 2014.

[34] J. Wilson and N. Patwari, "See-through walls: motion tracking using variance-based radio tomography networks," *IEEE Transactions on Mobile Computing*, vol. 10, no. 5, pp. 612–621, 2011.

[35] Y. J. Luo, J. G. Jiang, S. Y. Wang et al., "Filtering and cleaning for RFID streaming data technology based on finite state machine," *Journal of Software*, vol. 25, no. 8, 2014.